Parameterization of zero-skewness unpolarized GPDs

Hossein Vaziri[†] Mohammad Reza Shojaei[‡]

Department of Physics, Shahrood University of Technology, P. O. Box 36155-316, Shahrood, Iran

Abstract: Recent parameterizations of parton distribution functions (PDFs) have led to the determination of the gravitational form factors pertaining to the dependence of nucleons on their generalized parton distributions (GPDs) in the limit $\xi \to 0$. This study aims to obtain the flavor division of nucleon electromagnetic and gravitational form factors using the VS24 ansatz and two PDFs at the N^3LOapproximation in GPDs. The PDFs and GPD formalism enable the calculation of various form factors of nucleons in different approximations, as well as the calculation of the electric radius of nucleons. The study, despite its high approximation complexity, enhances the accuracy of calculations and aligns them more closely with experimental values.

Keywords: QCD-PDFs-GPDs, form factors, structure function of the nucleons, hadron

DOI: 10.1088/1674-1137/add923 **CSTR:** 32044.14.ChinesePhysicsC.49093101

I. INTRODUCTON

The study of quark and gluon-compound particles can provide details about the nature of strong interactions. The spatial and momentum distributions of constituents in a hadron are not fully understood due to theoretical and calculational limitations, primarily based on measurements [1]. Deep-inelastic scattering (DIS) and hard proton-proton high-energy collisions involve scattering through the partonic constituents of the hadron. A set of universal parton distribution functions (PDFs) is necessary to predict the rates of various processes. The distributions can be best determined through global fits to all available DIS and hard-scattering data, obtained at leading-order (LO), next-to-leading order (NLO), next-to-next-to-leading order (N^{2}LO), or next-to-next-to-next leading order (N^{3}LO) in the strong coupling α_s. Over the past few years, there has been a significant enhancement in the precision and kinematic range of experimental measurements for various processes, along with the emergence of new data types. The reliability of global analyses has been enhanced by significant theoretical developments [2].

Several research groups have previously studied PDFs [3–11]. The old form of describing the hadron structure, parton distributions, relied on the B-jorken longitudinal variable x, while more complex functions, generalized parton distributions (GPDs), depended on x, momentum transfer t, and skewness parameter ξ [12–15]. The unique characteristic of GPDs (x, ξ, t) is that the integration of different momenta of GPDs over x yields different hadron form factors such as electromagnetic form factors and gravitational form factors (GFFs) [16–18]. The x dependence of GPDs is primarily determined by standard PDFs, which are derived from deep-inelastic process analysis [19–21].

This section uses one ansatz that illustrates how x and t rely on GPDs [22]. We select two PDFs at the N^{3}LO approximation [23–25], combine them into our ansatz, and demonstrate a favorable agreement with experimental data for the calculation of form factors and radii of nucleons. Using GPDs, we can calculate the form factors as well as the radius of the nucleons. Thus, the remainder of this paper is organized as follows. In Sec. II, we introduce the PDFs. This section provides a comprehensive explanation of the general method and form of obtaining these functions. Sec. III includes GPDs and hadron form factors of nucleons, along with related remarks. This section also provides an explanation of the formalism of GPDs and the calculation method of form factors. The GFFs of the nucleons based on various Ansatsez and JHA21 PDFs at theN^{3}LO approximation [24, 25] are presented in Sec. IV. Sec. V presents the electric radii of nucleons using the combination of the VS24 ansatz [22] and JHA21 PDFs [24, 25]. The results and conclusions of our study are presented in Sec. VI.

II. PARTON DISTRIBUTION FUNCTIONS

PDFs are a necessary component in the calculation of particle cross-sections at collider experiments with hadron beams. The explanation of hard processes with one or

Received 21 February 2025; Accepted 15 May 2025; Published online 16 May 2025

[†] E-mail: Hossein.Vaziri@shahroodut.ac.ir

[‡] E-mail: Shojaei.ph@gmail.com

two hadrons in the initial state requires an understanding of PDFs. Knowledge of PDFs is necessary for the description of hard processes with one or two hadrons in the initial state (Fig. 1).

The cross section of a hadron in its initial state, as seen in deeply inelastic lepton scattering at HERA (Fig. 1), consists of the following form [26]:

$$\mathrm{d}\sigma \sim \sum_{a,b} \int \mathrm{d}x_A f_{a/A}(x_A,\mu)\mathrm{d}\widehat{\sigma}. \tag{1}$$

There exists a relationship between matrix elements of some local operators and the moments of the PDFs, which are present in the operator product expansion for deeply inelastic scattering. This relation can also be used as the definition [27, 28]. The technical definition of PDFs can now be studied. There are, in fact, two definitions in current use: the $\overline{\mathrm{MS}}$ definition, which is the most commonly used, and the DIS definition, in which deeply inelastic scattering plays a prominent role [26]. The resulting PDFs depend on the selected input data, the order in which the perturbative QCD computation is performed, the assumptions regarding the PDFs, the handling of heavy quarks, and the treatment of uncertainties. Presently, the determination of PDFs is being performed by several research groups, namely MSTW [2], CTEQ [29], NNPDF [30], HERAPDF [31], AB(K)M [32], and GJR [33]. According to the mentioned methods, PDFs are obtained, as a function of the average momentum fraction x. Usually, the form of these functions for the u and d quarks is as follows:

$$xu_v = A_u x^{\eta_1}(1-x)^{\eta_2}(1+\epsilon_u x^{\eta_3}+\gamma_u x), \tag{2}$$

$$xd_v = A_d x^{\eta_4}(1-x)^{\eta_5}(1+\epsilon_d x^{\eta_6}+\gamma_d x), \tag{3}$$

where the coefficients are obtained by fitting with the experimental data. For example, the JHA21 PDFs at the N^{3}LO approximation are as follows [24, 25]:

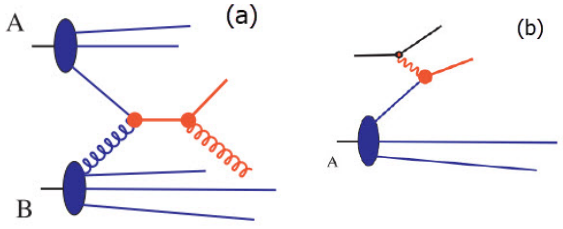

Fig. 1. (color online) a) $HadronA + HadronB \to 2Partons$ [26]. b) Deeply inelastic scattering [26].

$$xu_v = 0.261x^{0.298}(1-x)^{4.032}(1+6.042x^{0.5}+35.492x), \tag{4}$$

$$xd_v = 1.085x^{0.5}(1-x)^{5.921}(1-3.618x^{0.5}+16.414x). \tag{5}$$

The KKA10 PDFs at the N^{3}LO approximation are [23]

$$xu_v = 3.41356x^{0.298}(1-x)^{3.76847}(1+0.1399x^{0.5}-1.12x), \tag{6}$$

$$xd_v = 5.10129x^{0.79167}(1-x)^{4.02637}(1+0.09x^{0.5}+1.11x). \tag{7}$$

Figure 2 shows some examples of different PDF charts for different approximations.

III. GPDs AND HADRON FORM FACTORS

The hadron form factors are linked to the GPDs (x, ξ, t) using the following sum rules [6, 34]:

$$F_1(t) = \sum_q e_q \int_{-1}^{1} \mathrm{d}x H^q(x,t,\xi), \tag{8}$$

$$F_2(t) = \sum_q e_q \int_{-1}^{1} \mathrm{d}x E^q(x,t,\xi), \tag{9}$$

When the momentum is transverse and located in the space-like region, the value of ξ is equal to zero. In the range of $0 < x < 1$, the integration region can be reduced. By revising the elastic form factors, we obtain

$$F_1(t) = \sum_q e_q \int_{0}^{1} \mathrm{d}x \mathcal{H}^q(x,t,\xi=0), \tag{10}$$

$$F_2(t) = \sum_q e_q \int_{0}^{1} \mathrm{d}x \mathcal{E}^q(x,t,\xi=0), \tag{11}$$

In the limit $t \to 0$, the functions $H^q(x,t)$ decrease to usual quark densities in the proton:

$$\mathcal{H}^u(x,t=0) = u_v(x), \quad \mathcal{H}^d(x,t=0) = d_v(x), \tag{12}$$

with the integrals

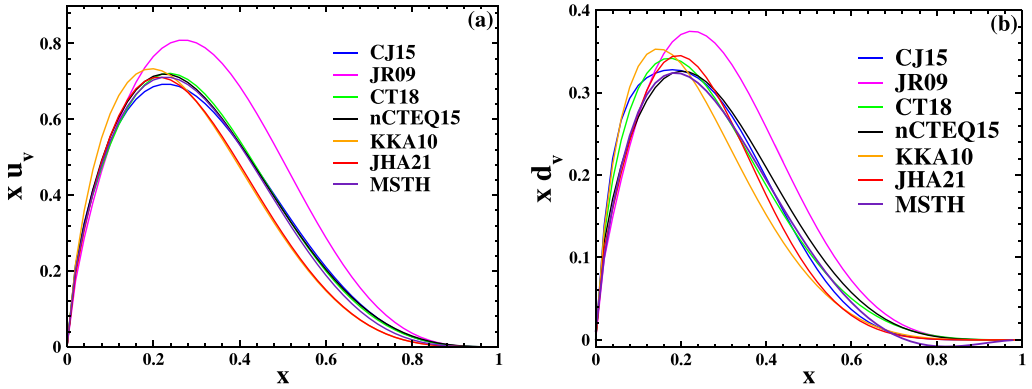

Fig. 2. (color online) xu_v and xd_v of the CJ15 PDFs at the NLO approximation [35]; JR09 PDFs [36] at the NNLO approximation; CT18 PDFs [37] at the NNLO approximation; and nCTEQ15 [38], KKA10 [23], JHA21 [24–25], and MSTH [39] PDFs at the NNNLO approximation as a function of x.

$$\int_0^1 u_v(x)\mathrm{d}x = 2, \quad \int_0^1 d_v(x)\mathrm{d}x = 1. \tag{13}$$

normalized to the proton's u and d valence quark numbers. These factors result in the determination of certain parameters. For instance, the values $\kappa_u = 1.673$ and $\kappa_d = -2.033$ are obtained. Moreover, the normalization integral for the mathematical constant $\int_0^1 \mathcal{H}_q(x,0)$ takes on particular values for the nucleons: $F_1^p(0) = 1$ for the proton and $F_1^n(0) = 0$ for the neutron.

The functions $\mathcal{H}(x)$ and $\varepsilon(x)$ differ in each of the models that have been suggested. To yield a faster reduction with t, the $x \to 0$ limit of $\varepsilon(x)$ should contain additional powers of $(1-x)$, compared with $\mathcal{H}(x)$ [6, 34, 40]. Hence, we have

$$\begin{aligned}\varepsilon_u(x) &= \frac{\kappa_u}{N_u}(1-x)^{\eta_u}u_v(x),\\ \varepsilon_d(x) &= \frac{\kappa_d}{N_d}(1-x)^{\eta_d}d_v(x),\end{aligned} \tag{14}$$

where the normalization factors N_u and N_d are determined as [6]

$$\begin{aligned}N_u &= \int_0^1 \mathrm{d}x(1-x)^{\eta_u}u_v(x),\\ N_d &= \int_0^1 \mathrm{d}x(1-x)^{\eta_d}d_v(x).\end{aligned} \tag{15}$$

The proton value must be $F_2^p(0) = \kappa_p = 1.793$, and the neutron value must be $F_2^n(0) = \kappa_n = -1.913$ to satisfy the limits on κ_q.

$$\kappa_q = \int_0^1 \mathrm{d}x\varepsilon_q(x). \tag{16}$$

$$\kappa_u = \kappa_n + 2\kappa_p, \quad \kappa_d = 2\kappa_n + \kappa_p. \tag{17}$$

One of the most important techniques for examining the structure of nucleons is the use of GPDs [27, 28, 41].

To satisfy the requirements outlined in Eq. (14), the nucleon form factor data were fitted to obtain the values of η_u and η_d. We must adjust our models to increase the agreement with the data for large $-t$.

The extended ER [6], modified Gaussian (MG) [34], HS22 [20], M-HS22 [19], and VS24 ansatzes [22] are among the ansatzes with a t dependency that are presented in this paper. In this section, we first introduce different ansatzes. The ER ansatz is [6]

$$\mathcal{H}^q(x,t) = q_v(x)x^{-\alpha'(1-x)t}, \tag{18}$$

$$\varepsilon_q(x,t) = \varepsilon_q(x)x^{-\alpha'(1-x)t}. \tag{19}$$

The MG ansatz is followed as [34]

$$\mathcal{H}^q(x,t) = q_v(x)\exp\left[\alpha\frac{(1-x)^2}{x^m}t\right], \tag{20}$$

$$\varepsilon_q(x,t) = \varepsilon_q(x)\exp\left[\alpha\frac{(1-x)^2}{x^m}t\right]. \tag{21}$$

The free parameters for the MG ansatz are $m = 0.45$ and $\alpha = 1.15$, and for the extended ER, $\alpha' = 1.09$.

We have introduced the HS22 and M-HS22 ansatzes in Refs. [20] and [19], respectively, which have more parameters than the ER and MG ansatzes.

We vary our previous M-HS22 ansatz [19] for the GPDs by adding two new parameters, m'' and γ, and introduce the VS24 ansatz [22], which is as follows:

$$\mathcal{H}_q(x,t) = q_v \exp[-\alpha'''t(1-x)^{\gamma}\ln(x)+\beta x^{m'}\ln(1-bt)], \quad (22)$$

$$\varepsilon_q(x,t) = \varepsilon_q(x) \exp[-\alpha'''t(1-x)^{\gamma}\ln(x)+\beta x^{m'}\ln(1-bt)], \quad (23)$$

Using the VS24 ansatz in combination with the KKA10 [23] and JHA21 [23–25] PDFs, we calculate the form factors of the u and d quarks based on the formalism described earlier.

The Dirac and Pauli form factors of the u and d quarks that are obtained using the KKA10 [23] and JHA21 PDFs [24, 25] are shown in Fig. 3 and Fig. 4, respectively, as functions of $-t$. The parameters of these PDFs are listed in Table 1. By combining five different types of ansatzes with two PDFs, the form factors of the u and d quarks are calculated.

As is evident from these figures, the form factors obtained from the VS24 ansatz [22] combined with JHA21 PDFs [24, 25] show better agreement with the form factors obtained from electron-proton inelastic scattering experiments [43–45] than those obtained with KKA10 PDFs [23].

The proton and neutron Dirac form factors are defined as

$$F_1^p(t) = e_u F_1^u(t) + e_d F_1^d(t), \quad (24)$$

$$F_1^n(t) = e_d F_2^u(t) + e_d F_2^d(t). \quad (25)$$

Therefore, the Pauli form factors are

$$F_2^p(t) = e_u F_2^u(t) + e_d F_2^d(t), \quad (26)$$

$$F_2^n(t) = e_d F_2^u(t) + e_u F_2^d(t). \quad (27)$$

where $e_u = 2/3$ and $e_d = -1/3$ are the corresponding quark electric charges. As a result, the t-dependence of the GPDs $(x, \xi = 0, t)$ can be determined from the analysis of the nucleon form factors for which experimental data exist in a wide region of momentum transfer.

The form factors of nucleons are plotted as a function of $-t$ in Fig. 5; their calculations are obtained from the combination of the VS24 ansatz [22] and different PDFs.

The Sachs form factors can be derived from $F_1(t)$ and $F_2(t)$ in the following manner [6, 46, 48]:

$$G_E^N(t) = -\tau F_2(t) + F_1(t), \quad G_M^N(t) = F_2(t) + F_1(t). \quad (28)$$

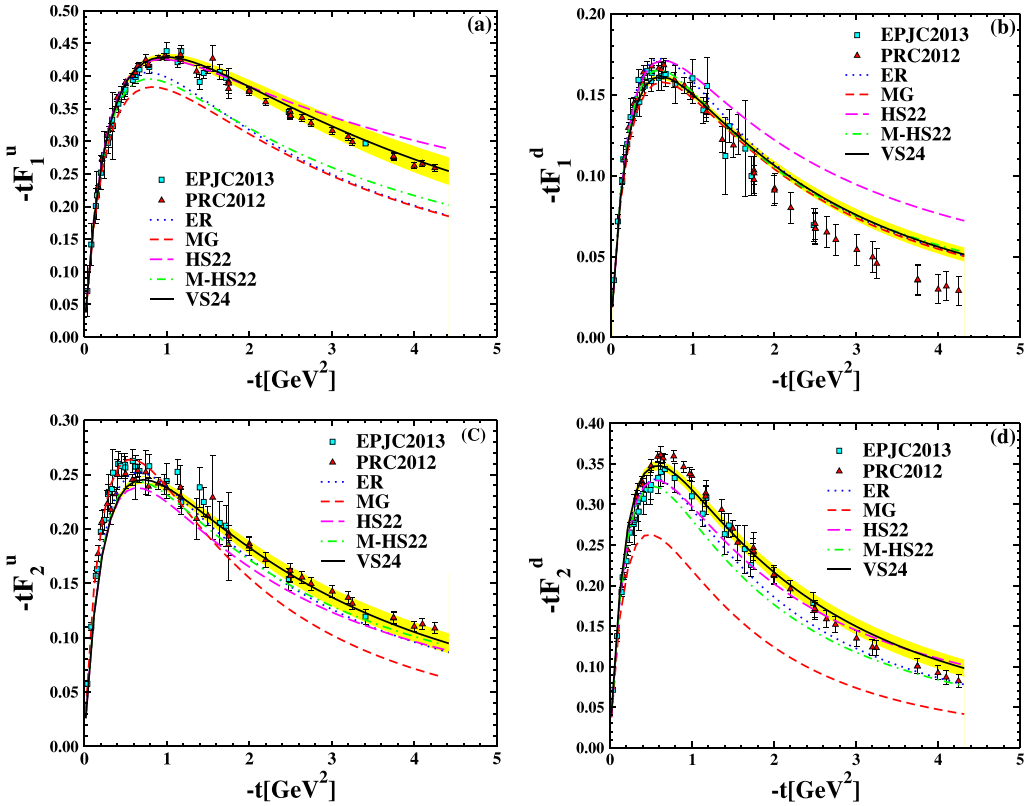

Fig. 3. (color online) $F_1^{u,d}$ and $F_2^{u,d}$ are multiplied by t as a function of $-t$. Comparison of the ER [6], MG [34], HS22 [20], and M-HS22 [19] ansatzes with the VS24 ansatz [22]. All these utilize the KKA10 PDF [23]. Experimental data from [43] (triangle up), [44] (circle), and [45] (square) serve as a basis for the extracted points.

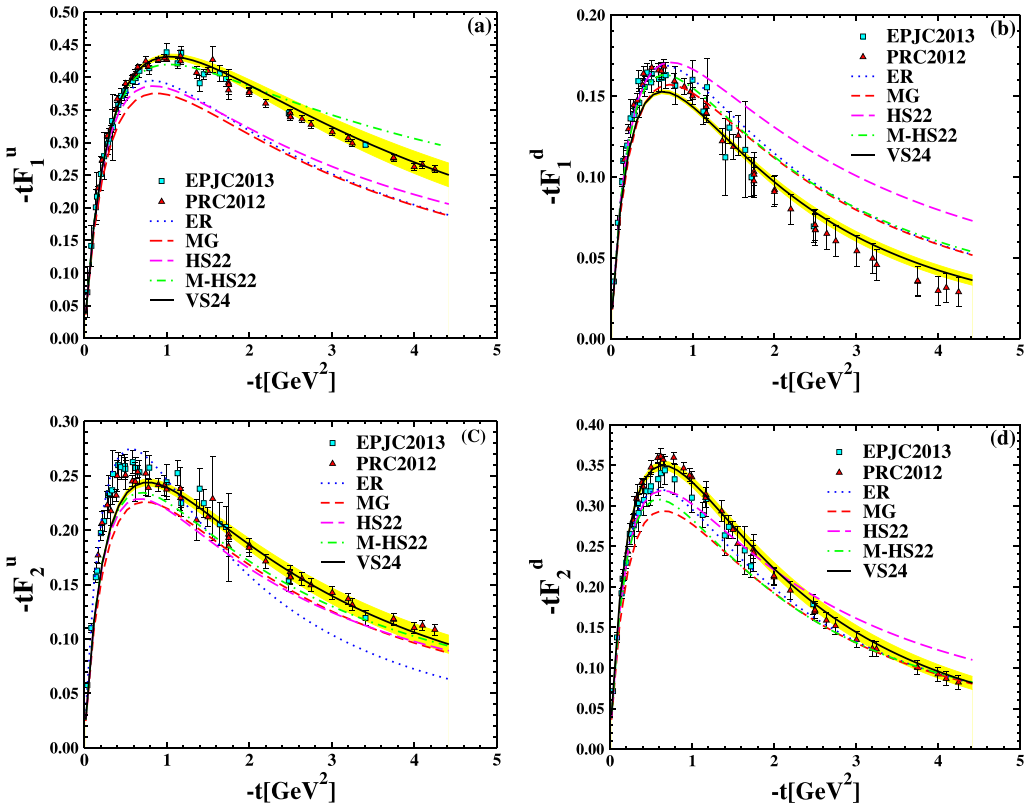

Fig. 4. (color online) $F_1^{u,d}$ and $F_2^{u,d}$ are multiplied by t as a function of $-t$. Comparison of the ER [6], MG [34], HS22 [20], and M-HS22 ansatzes [19] with the VS24 ansatz [22]. All these utilize the JHA21 PDF [24–25]. The extracted points are based on experimental data from [43] (triangle up), [44] (circle), and [45] (square).

Table 1. Coefficients for calculations of Eqs.(22) and (23). We use the VS24 ansatz [22]. The parameters b and m' are fixed; the others are calculated by fitting.

	KKA10 PDFs [23]	JHA21 PDFs [24–25]
α''	$1.3742 \pm 7.16734 \times 10^{-3}$	$1.3473 \pm 7.18952 \times 10^{-3}$
β	$1.52378 \pm 2.8392 \times 10^{-2}$	$1.51418 \pm 2.5564 \times 10^{-2}$
γ	$0.0570108 \pm 1.49425 \times 10^{-2}$	$2.9823 \pm 1.2596 \times 10^{-2}$
η_u	$0.71207 \pm 9.909 \times 10^{-3}$	$0.6931 \pm 9.8663 \times 10^{-3}$
η_d	$0.19248 \pm 1.606 \times 10^{-2}$	$0.2782 \pm 1.7735 \times 10^{-2}$
b	2	2
m'	0.65	0.65

where $t = Q^2$ is the four-momentum transfer of the virtual photon, and $\tau \equiv -t/4M_N^2$. Sach suggests that the form factors G_E and G_M may have a more fundamental significance compared to F_1 and F_2 in interpreting the spatial distributions of charge and magnetization inside the nucleon, as they are related to the four-momentum transfer of the virtual photon [46].

Since the errors in F_1 and F_2 are typically more correlated and larger compared to the errors in G_E and G_M, we study G_E and G_M for nucleons. There are differences between the down- and up-quark distributions [47]:

$$G^p_{E,M}(Q^2) = \frac{2}{3}G^u_{E,M}(Q^2) - \frac{1}{3}G^d_{E,M}(Q^2), \tag{29}$$

$$G^n_{E,M}(Q^2) = \frac{2}{3}G^d_{E,M}(Q^2) - \frac{1}{3}G^u_{E,M}(Q^2). \tag{30}$$

The form factors in the combination of the VS24 ansatz [22] and JHA21 PDFs [24, 25] are compared to those obtained from scattering experiments for the Rosenbluth equation at $q^2 = 0$, as summarized in Table 2.

Studying the contributions of up and down quarks to the form factors of the nucleon can provide insights into its fundamental structure and dynamics [49]. Figure 6 shows the electric and magnetic form factors of the nucleons, derived from JHA21 PDFs [24, 25] and plotted as functions of $-t$.

This graph shows that the form factors obtained from the combination of the VS24 ansatz [22] and JHA21 PDFs [24, 25] are more consistent with experimental data [43–45] than other combinations of the ansatzes with JHA21 PDFs [24, 25]. In particular, for G_E^n, the form factors are even better than those calculated by the combination of the VS24 ansatz and KKA10 PDFs in Ref. [22].

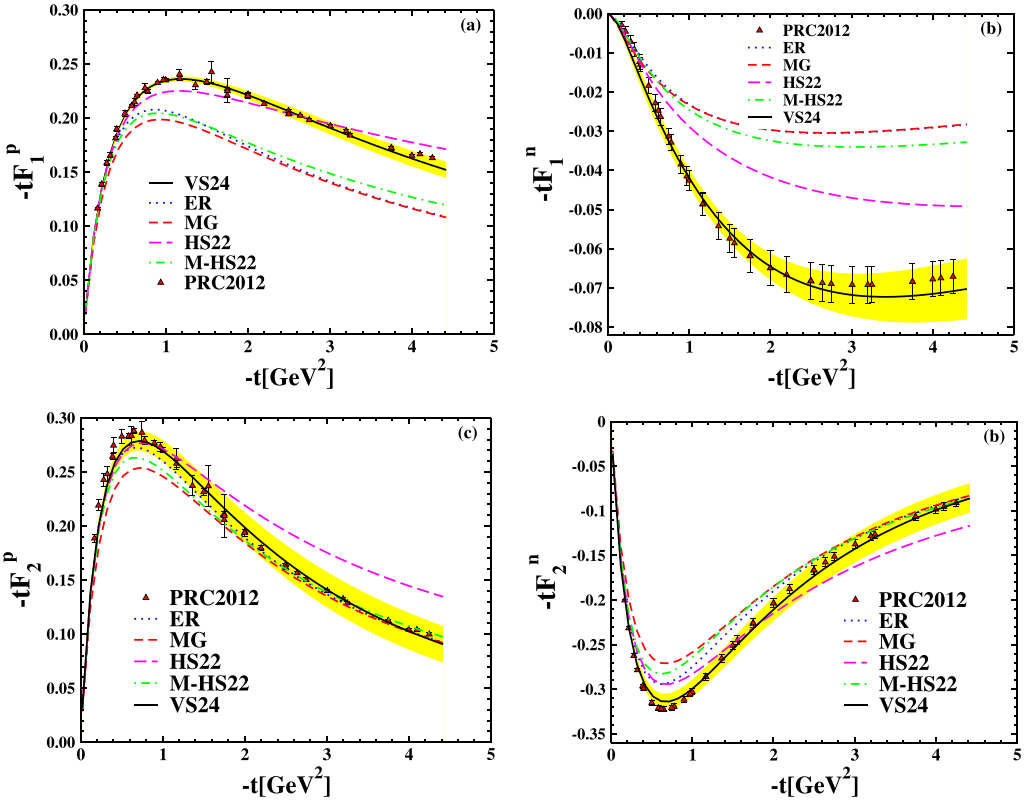

Fig. 5. (color online) $F_1^{p,n}$ and $F_2^{p,n}$ are multiplied by t as a function of $-t$. Comparison of the ER [6], MG [34], HS22 [20], M-HS22 [19], and VS24 ansatzes [22]. All these utilize the JHA21 PDF [24, 25]. The extracted points are based on experimental data from [43] (triangle up), [44] (circle), and [45] (square).

IV. GRAVITATIONAL FORM FACTORS OF NUCLEONS (QUARK AND GLUON CONTRIBUTIONS)

There are four GFFs of the proton: $A(q^2)$, $B(q^2)$, $C(q^2)$, and $\bar{C}(q^2)$. The GFFs $A(q^2)$ and $B(q^2)$ are related to the mass and angular momentum distributions of the proton. Conservation of the energy-momentum tensor constrains the GFFs $A(q^2)$ and $B(q^2)$, and $\bar{C}(q^2)$; however, $C(q^2)$, also known as the D-term, is not related to any Poincare generator and is unconstrained by such conservation laws. The D-term contributes to the DVCS process when the skewness ξ is nonzero or when there is a longitudinal momentum transfer from the initial state proton to the final state proton [51]. Taking the matrix elements of the energy-momentum tensor $T_{\mu\nu}$ instead of the electromagnetic current J^{μ}, one can obtain the GFFs of quarks, which are related to the second rather than the first moments of GPDs [52]:

$$A_q(t) = \int_{-1}^{1} \mathrm{d}x\, x\, H^q(x,t,\xi), \tag{31}$$

$$B_q(t) = \int_{-1}^{1} \mathrm{d}x\, x\, E^q(x,t,\xi). \tag{32}$$

Table 2. Values of $G_{E,M}^{p}$ and $G_{E,M}^{n}$ at $t=0$.

$G_{E,M}^{P,n}(0)$	EXP.DATA [50]	JHA21 [24, 25]+VS24 [22]
$G_E^p(0)$	1	1
$G_M^p(0)$	+2.79	+2.65867
$G_E^n(0)$	0	3.2×10^{-13}
$G_M^n(0)$	−1.91	−1.94332

For $\xi = 0$, the valence contribution to the gravitational form factor is as follows:

$$A_q(t) = \int_0^1 \mathrm{d}x x H^q(x,t), \tag{33}$$

$$B_q(t) = \int_0^1 \mathrm{d}x x E^q(x,t). \tag{34}$$

This representation, combined with our model (we use here the first variant of parameters describing the experimental data obtained by the polarization method), allows us to calculate the GFFs of valence quarks and their contribution (being just their sum) to GFFs of nucleons. The t dependency of $A_{u+d}(t)$ is the same for our GPDs with varying PDFs. These contributions add up to

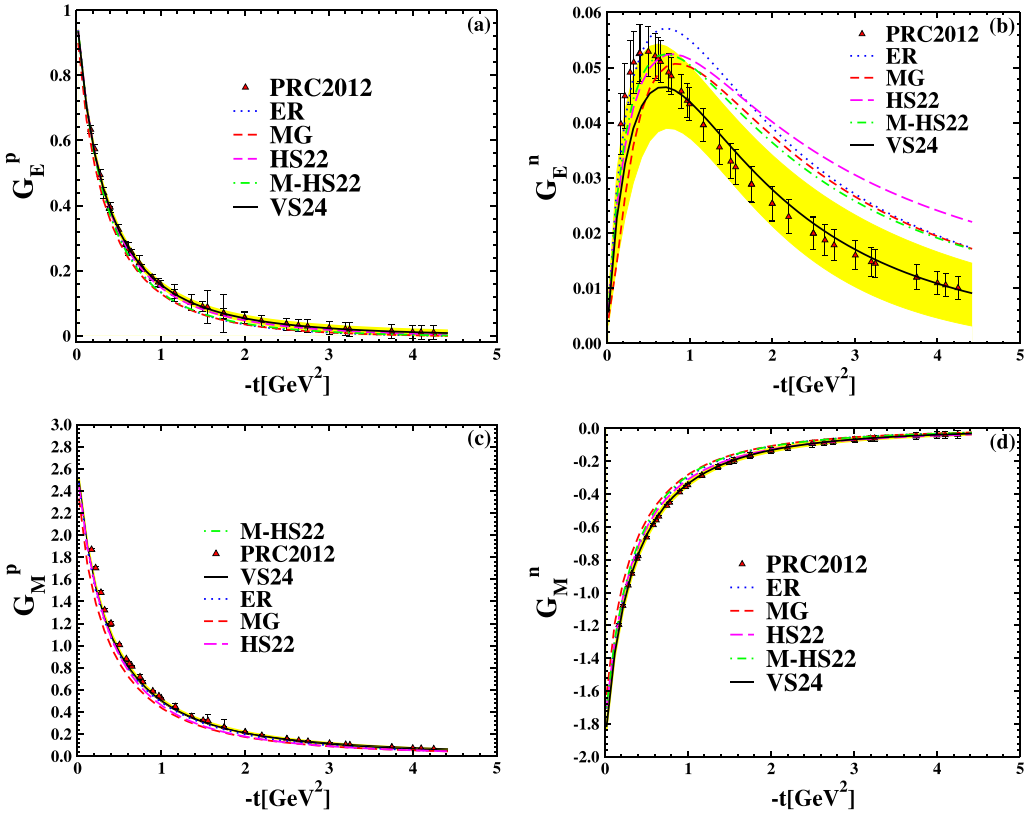

Fig. 6. (color online) $G_E^{p,n}$ and $G_M^{p,n}$ as a function of $-t$. Comparison of the ER [6], MG [34], HS22 [20], M-HS22 [19], and VS24 ansatzes [22]. All these utilize the JHA21 PDF [24, 25]. The extracted points are based on experimental data from [43] (triangle up).

$A_{u+d}(t) \approx 0.45$ at $t = 0$.

The values corresponding to various PDFs are given in Table 3.

The PDFs are as follows: the CJ15 PDFs in the NLO approximation [35], the JR09 PDFs in the NNLO approximation [36], CT18 PDFs in the NNLO approximation [37], nCTEQ15 PDF in the NNLO approximation [38], KKA10 PDF in the NNNLO approximation [23], JHA21 PDF in the NNNLO approximation [24, 25], and MSTH PDF in the NNNLO approximation [39]. Combining these PDFs with the VS24 ansatz [22], we calculated the GFFs for u and d quarks and plotted them as a function of $-t$. Fig. 7 shows a comparison of the proton GFF A_{u+d} as a function of $-t$ for MMNS (Lattice QCD) [51] with the JHA21 PDF in the NNNLO approximation [24, 25], utilizing the VS24 ansatz [22]. In Fig. 8, we also present the calculations of A^u for the GJLY group [42] and plot the corresponding form factors. It can be seen that the behaviors of all graphs of GFFs are similar when combining these PDFs with the desired ansatz.

V. ELECTRIC RADII OF NUCLEONS BASED ON VS24 ANSATZ

The particle radii at zero momentum transfer are determined by the slope of form factors, and the squares of the Dirac radius $< r_D^2 >$ and charge radius $r_{E,p}^2$ are determined using the following method [53]:

$$< r_D^2 > = -6 \frac{\mathrm{d}F_1^{p,n}(t)}{\mathrm{d}t}\bigg|_{t=0},$$
$$< r_E^2 > = -6 \frac{\mathrm{d}F_1^{p,n}(t)}{\mathrm{d}t}\bigg|_{t=0} + \frac{3}{2}\frac{\kappa_{n,p}}{m_{n,p}^2}. \quad (35)$$

In addition, we used the VS24 ansatz [22] to compute the nucleon's Dirac mean squared radii.

Table 3. Exact values of $A_{u+d}(t)$ for different PDFs at $t = 0$. All these use the VS24 ansatz [22].

PDFs	$A_{u+d}(t)$
CJ15 [35]	0.455512
JR09 [36]	0.455512
CT18 [37]	0.459818
nCTEQ15 [38]	0.46219
KKA10 [23]	0.43291
JHA21 [24, 25]	0.425903
MSTH [39]	0.44496

$$< r^2_{D,p} >= -6\alpha''' \int_0^1 \mathrm{d}x[e_u u_v(x) + e_d d_v(x)](1-x)^\gamma \times \ln(x) + \beta x^{m'} \ln(1-bt)\,|_{t=0}, \quad (36)$$

$$< r^2_{D,n} >= -6\alpha''' \int_0^1 \mathrm{d}x[e_u d_v(x) + e_d u_v(x)](1-x)^\gamma \times \ln(x) + \beta x^{m'} \ln(1-bt)\,|_{t=0}\,. \quad (37)$$

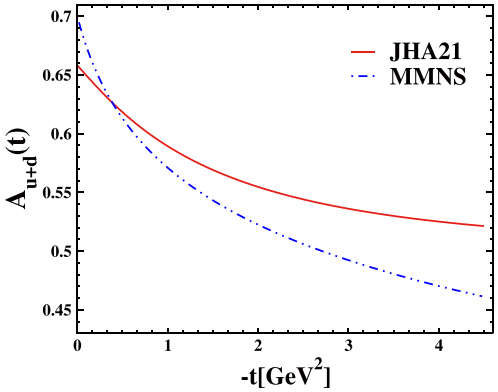

Fig. 7. (color online) Proton GFF A_{u+d} as a function of $-t$. The JHA21 PDF in the NNNLO approximation [24, 25], combined with the VS24 ansatz [22]. The results of MMNS (Lattice QCD) [51] are plotted.

The proton charge radius is defined as the slope of the electric form factor in the forward limit ($t = 0$), and therefore, it does not depend on $-t$. In Table 4, we list the calculated electric radii of nucleons using the JHA21 PDFs [24, 25] combined with the VS24 ansatz [22] and compare them with experimental data obtained from [54].

Table 4. Proton electric radii calculated using the JHA21 PDFs [24, 25] and VS24 model [22]. Ref. [54] is the source of the data.

Ansatz+PDFs	$r_{E,p}$
Exprimental data [54]	0.831 fm
VS24 [22]+JHA21 [24–25]	0.853154 fm

VI. RESULTS AND CONCLUSION

This study examines a collection of parameteriza-

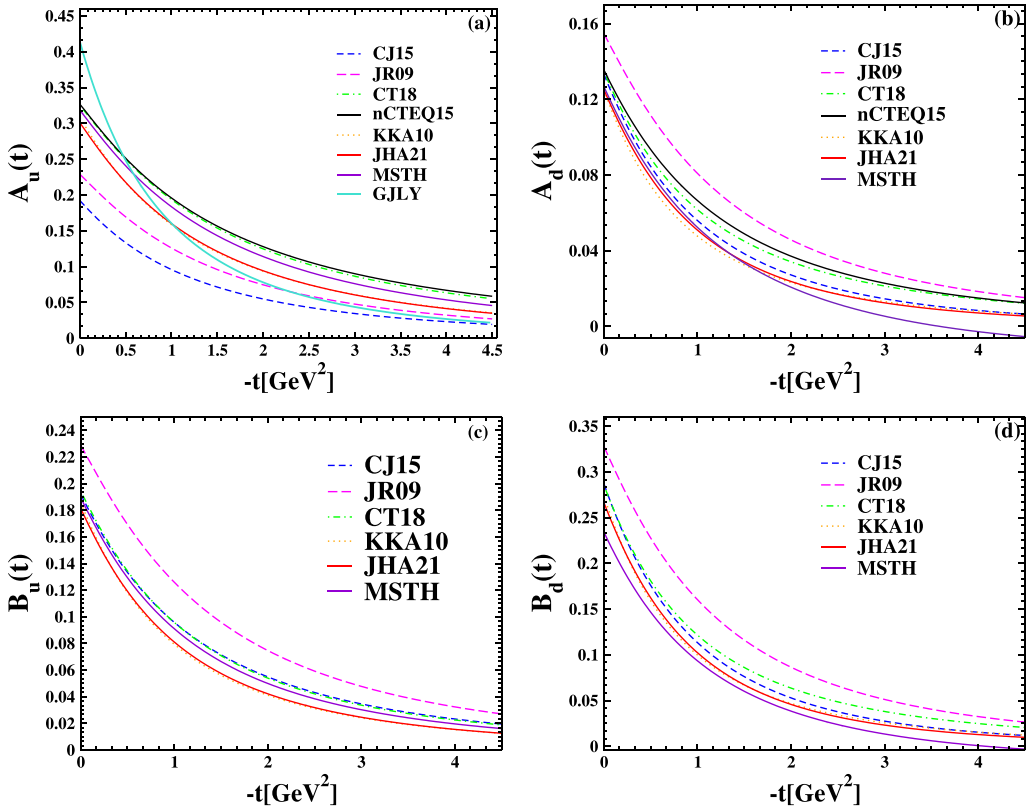

Fig. 8. (color online) $A^{u,d}$ and $B^{u,d}$ as a function of $-t$. The CJ15 PDFs in the NLO approximation [35], JR09 PDFs in the NNLO approximation [36], CT18 PDFs in the NNLO approximation [37], nCTEQ15 PDF in the NNLO approximation [38], KKA10 PDF in the NNNLO approximation [23], JHA21 PDF in the NNNLO approximation [24, 25], and MSTH PDF in the NNNLO approximation [39], combined with the VS24 ansatz [22]. The GFF of GJLY [42] is plotted.

tions of the zero-skewness unpolarized quark GPDs, H and E, with flavor separation between u and d quarks. The parameterizations are constructed using several PDF extractions and fitted to elastic form factor datasets. GFFs are then derived. PDFs are functions that only depend on x B-jorken (indicating the average longitudinal momentum fraction of the partons). These functions are obtained using inelastic scattering data of electrons from protons. However, GPDs depend on t and ξ, in addition to x: t is the momentum transfer, and ξ measures the longitudinal momentum transfer in hard scattering. The basis of our study is the calculation of the form factors of nucleons, of which quarks are also a part. By calculating the electric, magnetic, and gravitational form factors, we can study the structural aspects of nucleons such as radius and density. We start with the introduction of PDFs and their formalism in Sec. II and explain the method of obtaining these functions using the dispersion relation. The general form of these functions is expressed in Eqs. (2) and (3), and some examples of different PDF charts as a function of x at different approximations are shown in Fig. 2. The figures indicate that the behavior and physics of these functions are the same. Since GPDs represent the space inside the nucleons in three dimensions, we discuss GPDs and form factors in Sec. III. Subsequently, we explain the formalism of GPDs in detail via Eqs. (8)–(16), where F_1 and F_2 are the Pauli and Dirac form factors, respectively. In fact, $H^q(x,t,\xi=0)$ and $E^q(x,t,\xi=0)$ have two parts: the first part is the PDF, and the other is a proposed function extracted by fitting with form factors obtained from scattering experiments, using data from Refs. [43−45]. The proposed ansatz is a function that is usually exponential, and the most important ansatzes are as follows: ER [6], MG [34], HS22 [20], M-HS22 [19], and VS24 [22]. The PDFs used in GPDs are also different; here, we use the JHA21 PDFs at the N^{3}LO approximation [24–25]. With these explanations, we plot the form factors for u and d quarks in Fig. 4; the form factor diagrams for the JHA21 PDFs, especially for F_1^d, are more consistent with the experimental data than those for the KKA10 PDFs [23], as evident from comparing Figs. 3 and 4. We obtained these coefficients by fitting data from [43−45]. The diagrams in Fig. 5 depict nucleon form factors as a function of $-t$, calculated using the JHA21 PDFs [24–25] and various ansatsez. $G_E^{p,n}$ and $G_M^{p,n}$ as a function of $-t$ are shown in Fig. 6. The analysis shows that, especially for the neutron's electric form factors, the JHA21 PDFs are more consistent with experimental data than the KKA10 PDFs. Eq. (28) was used to arrive at this conclusion. In each figure presented in this paper, we have analyzed the parameters of the VS24 ansatz for the upper and lower limits. Furthermore, using the necessary ansatz, we computed the form factors at $q^2=0$ and compared them with the form factors derived from the experimental data of Ref. [50]. Table 2 lists the results of the computation. In general, it is difficult to find constant coefficients to fit all the electric and magnetic form factors of quarks as well as nucleons with the form factors obtained from DIS experiments. However, Figs. 3−6 show that the coefficients introduced in Table 2 are suitable for the VS24 ansatz and JHA21 PDFs. In Sec. IV, we discussed GFFs$A_q(q^2)$ and $B_q(q^2)$, representing another application of GPDs. By combining the different PDFs and VS24 ansatz, we calculated the form factors using Eqs. (32)−(34) and then plotted them in Fig. 8. Considering that there are no experimental data for GFFs, we see that the behaviors of all graphs in this figure are the same. Moreover, at$t=0$, when using different PDF combinations with the VS24 ansatz to calculate the form factors, the obtained $A_{u+d}(t)$ values are almost the same, as evident in Table 3. In addition, the proton GFF A_{u+d} as a function of $-t$ for the MMNS (Lattice QCD) [51] is plotted in Fig. 7. Measuring the electric radii of protons and neutrons is a significant application of form factors; therefore, in Sec. V, we discuss the radii of nucleons. Eqs. (35)−(37) are used to compute the Dirac mean squared radii of the nucleon using the VS24 model. Table 4 lists the outcomes of these computations for the VS24 ansatz and JHA21 PDFs. The parameters that were selected for the VS24 ansatz match the data used in Ref. [54]. A comprehensive comparison was made between the results of this ansatz and PDFs in the N^{3}LO approximation. Given that we are working with a combination of PDFs and ansatzes, the VS24 ansatz was introduced to fit the experimental data. This ansatz was then combined with other PDFs, including the JHA21 PDFs, and it was determined that the combination of the VS24 ansatz and JHA21 PDFs better matches the experimental data. The optimal combination (among all listed combinations) was achieved using additional ansatzes. Further, the results of two groups, GJLY [42] and MMNS (Lattice QCD) [51], are plotted. Both the proton and neutron form factors obtained with this combination were satisfactory.

References

[1] I. Abt *et al.*, Phys. Rev. D **106**, 079901 (2022)

[2] R. S. Thorne, A. D. Martin, W. J. Stirling *et al.*, Eur. Phys. J. C **63**, 189 (2009)

[3] F. Halzen and A. D. Martin, *Quarks & Leptons* (Wiley, New York, 1984)

[4] P. Masjuan, E. R. Arriola, and W. Broniowski, EPJ Web Conf. **73**, 04021 (2014)

[5] M. N. Rosenbluth, Phys. Rev. D **79**, 079615 (1950)

[6] M. Guidal, M. V. Polyakov, A. V. Radyushkin *et al.*, Phys. Rev. D **72**, 054013 (2005)

[7] M. Reza Shojaei, Eur. Phys. J. A **52**(4), 111 (2016)
[8] M. Burkardt, Int. J. Mod. Phys. A **18**, 173 (2003)
[9] G. A. Miller, B. M. K. Nefkens, and I. Slaus, Phys. Rept. **194**, 1 (1990)
[10] M. Guidal, H. Moutarde, and M. Vanderhaeghen, Rept. Prog. Phys. **76**, 066202 (2013)
[11] A. V. Radyushkin, Phys. Rev. D **83**, 076006 (2011)
[12] H. Hashamipour, M. Goharipour, K. Azizi *et al*., Phys. Rev. D **105**(5), 054002 (2022)
[13] O. V. Selyugin and O. V. Teryaev, Phys. Atom. Nucl. **87**(4), 518 (2024)
[14] N. S. Nikkhoo and M. R. Shojaei, Phys. Rev. C **97**(5), 055211 (2018)
[15] H. H. Hosseini Mojeni and M. R. Shojaei, Eur. Phys. J. Plus **137**(8), 938 (2022)
[16] D. Muller, D. Robaschik, B. Geyer *et al*., Fortsch. Phys. **42**, 101 (1994)
[17] X. D. Ji, Phys. Rev. Lett. **78**, 610 (1997)
[18] A. V. Radyushkin, Phys. Rev. D **56**, 5524 (1997)
[19] H. Vaziri and M. Reza Shojaei, Phys. Rev. C **107**(5), 055204 (2023)
[20] H. H. H. Mojeni and M. R. Shojaei, Phys. Rev. C **105**(2), 025202 (2022)
[21] N. S. Nikkhoo and M. R. Shojaei, Int. J. Mod. Phys. E **24**(11), 1550086 (2015)
[22] H. Vaziri and M. R. Shojaei, Eur. Phys. J. Plus. **139**(10), 905 (2024)
[23] A. N. Khorramian, H. Khanpour, and S. A. Tehrani, Phys. Rev. D **81**, 014013 (2010)
[24] J. Blumlein, H. Bottcher, and A. Guffanti, Nucl. Phys. B **774**, 182 (2007)
[25] J. Blümlein and M. Saragnese, Phys. Lett. B **820**, 136589 (2021)
[26] D. E. Soper, Nucl. Phys. B Proc. Suppl. **53**, 69 (1997)
[27] M. Diehl, Phys. Rept. **388**, 41 (2003)
[28] N. S. Nikkhoo and M. R. Shojaei, Nucl. Phys. A **969**, 138 (2018)
[29] P. M. Nadolsky, H. L. Lai, Q. H. Cao *et al*., Phys. Rev. D **78**, 013004 (2008)
[30] R. D. Ball *et al*., Nucl. Phys. B **809**, 1 (2009), arXiv: 0808.1231[hep-ph]
[31] F. D. Aaron *et al*., JHEP **01**, 109 (2010)
[32] S. Alekhin, J. Blumlein, S. Klein *et al*., Phys. Rev. D **81**, 014032 (2010)
[33] J. E. M. Aguilar, Eur. Phys. J. C **53**, 133 (2008)
[34] O. V. Selyugin and O. V. Teryaev, Phys. Rev. D **79**, 033003 (2009)
[35] A. Accardi, L. T. Brady, W. Melnitchouk *et al*., Phys. Rev. D **93**(11), 114017 (2016)
[36] P. Jimenez-Delgado and E. Reya, Phys. Rev. D **79**, 074023 (2009)
[37] T. J. Hou, J. Gao, T. J. Hobbs *et al*., Phys. Rev. D **103**(1), 014013 (2021)
[38] K. Kovarik, A. Kusina, T. Jezo *et al*., Phys. Rev. D **93**(8), 085037 (2016)
[39] J. McGowan, T. Cridge, L. A. Harland-Lang *et al*., Eur. Phys. J. C **83**, 185 (2023)
[40] H. H. H. Mojeni and M. R. Shojaei, J. Exp. Theor. Phys. **131**(6), 910 (2020)
[41] M. R. Shojaei and N. S. Nikkhoo, Nucl. Phys. A **943**, 137 (2015)
[42] Y. Guo, X. Ji, Y. Liu *et al*., Phys. Rev. D **108**(3), 034003 (2023)
[43] I. A. Qattan and J. Arrington, Phys. Rev. C **86**, 065210 (2012)
[44] G. D. Cates, C. W. de Jager, S. Riordan *et al*., Phys. Rev. Lett. **106**, 252003 (2011)
[45] M. Diehl and P. Kroll, Eur. Phys. J. C **73**(4), 2397 (2013)
[46] F. J. Ernst, R. G. Sachs, and K. C. Wali, Phys. Rev. **119**, 1105 (1960)
[47] S. D. Drell and T. M. Yan, Phys. Rev. Lett. **24**, 181 (1970)
[48] N. S. Nikkhoo and M. R. Shojaei, Int. J. Mod. Phys. A. **32**(17), 1750097 (2017)
[49] D. H. Beck and R. D. McKeown, Ann. Rev. Nucl. Part. Sci. **51**, 189 (2001)
[50] G. Hohler, E. Pietarinen, I. S. Stefanescu *et al*., Nucl. Phys. B. **114**, 505 (1976)
[51] J. More, A. Mukherjee, S. Nair *et al*., Phys. Rev. D **105**(5), 056017 (2022)
[52] A. G. Martin-Caro, M. Huidobro, and Y. Hatta, Phys. Rev. D. **108**(3), 034014 (2023)
[53] O. Selyugin, EPJ Web Conf. **222**, 03018 (2019)
[54] W. Xiong, A. Gasparian, H. Gao *et al*., Nature **575**, 147 (2019)